PHILOSOPHICAL MAGAZINE B, 1995, VOL. 71, NO. 3, 291–310

Preferred structures in small particles

By N. DORAISWAMY and L. D. MARKS
Department of Materials Science and Engineering,
Northwestern University, Evanston, Il 60208, USA

[*Received 1 July 1994 and accepted 29 July 1994*]

ABSTRACT

Morphological transformations of Au particles supported on SiO were observed by real-time high-resolution electron microscopy, and the data were analysed quantitatively to extract the relative probabilities of the different morphologies and compared with a probability model to understand the role of the different parameters that affect the transformations. The experimental data and probability model show good agreement and reveal several interesting trends for the first time. The single crystal population dominates over the icosahedral multiply twinned particles (Ic) and the decahedral multiply twinned particles (Dc) over the observed size regime 2–8 nm. The Ic shows a maximum in relative probability of occurrence at smaller sizes, whereas the Dc probability increases with size, leading to a transition region centred at 6·5 nm particle diameter at which Dc and Ic show almost equal relative probabilities. The activation energies of the morphologies are also affected by the surface stress and anisotropy of the surface free energies.

§ 1. INTRODUCTION

Small particles and clusters have been the focus of numerous studies during the last three decades. During this time several novel and interesting properties of these materials have been discovered. One such interesting property is the propensity of small particles to twin and form a variety of structures. The most common among the twinned structures is the class of multiply twinned particles (MTPs) comprising icosahedral (Ic) and decahedral (Dc) MTPs. First discovered and analysed during studies on the early stages of epitaxial nucleation and growth (Ino 1966, Allpress and Sanders 1967), they are now known to occur in all f.c.c. metals and materials such as germanium (Saito, Yatsuya, Mihama and Uyeda 1979, Dahmen and Westmacott 1986, Hofmeister, Bardamid, Junghanns and Nepijko 1991) and diamond (Badzian, Badzian, Roy, Messier and Spear 1988). In the most commonly accepted model Ics and Dcs are considered to be assemblies of single-crystal tetrahedra with (111) facets and twin related on their adjoining faces. Five tetrahedral units with two twin boundaries each, assembled about a common axis, form the Dc, and 20 tetrahedral units with a common vertex and three twin boundaries each form the Ic. An alternative model, often used in high-resolution electron microscopy image simultations (Barry, Bursill and Sanders 1985, Gai, Goringe and Barry 1986, Buffat, Flueli, Spycher, Stadelmann and Borel 1991), treats the Ics and Dcs as structures with distorted body centred orthorhombic (Mackay 1962, Yang 1979, Yang, Yacaman and Heinemann 1979, Schabes-Retchkiman, Gomez, Vazquez-Polo and Jose-Yacaman 1984) and rhombohedral point group symmetries, respectively (Bagley 1965, Yang 1979, Yang *et al.* 1979, Schabes-Retchkiman *et al.* 1984). Investigations of the thermdynamic stability of MTPs with respect to single crystals (Scs) using computer

simulations (Hoare and Pal 1971, Berry 1990, Cleveland and Landman 1991) and elastic theory (Ino 1969) reveal that Ics are more stable than Scs at smaller sizes. A modified Wulff construction approach (Howie and Marks 1984), allowing for a general analysis of the surface thermodynamics of small particles, placed the stability of Dcs as intermediate to that of Scs and Ics. Based only on the thermodynamics of the particles, Ics and Dcs would be absent at larger sizes; however, experimental observations show that the MTPs persist to sizes as large as 1-2 mm (Haluska, Kuzmany, Vybornov, Rogi and Fejdi 1993). A possible explanation for the deviation is that the particles are frozen in a kinetic state which allows the metastable phases to coexist with the lowest energy Sc. This would imply a gradual decrease in the number density of the MTPs with size. Again, experimental results do not reflect this trend (Solliard, Buffat and Faes 1976). An alternative mechanism of growth of MTPs, proposed by Gillet (Gillet and Gillet 1972) suggests that MTP growth proceeds by a layer-by-layer growth around the existing nuclei of MTPs. A similar model (Farges, de Feraudy, Raoult and Torchet 1983, 1984) interprets the growth of an Ic as a process which could proceed either by the formation of an extra f.c.c. layer by the adatoms taking up the normal f.c.c. positions, or by the formation of an extra layer corresponding to a twin. Yet another model (Iijima 1987) assumes the initial formation of a liquid droplet on which a Dc nucleates and subsequently grows into a Dc along the pentagonal symmetry axes. Mackay (1962) and Marks (1980) suggested that small particle structures are crystallographically inter-related, and thermal vibration modes can induce structural transformations between various existing single crystals and MTPs. In studies of small cobalt particles, Tholen (1981) illustrates a mechanism of martensitic transformations arising from a build-up of internal strain within the particles as a possible source of twinning. In fact, computer simulations of clusters (Hoare and Pal 1971, Berry 1990) have shown that the energy differences between MTPs and Scs are very small and clusters need not have a single stable structure, but can have a multiplicity of configurations.

Real-time imaging of the structural transformations in small particles by Iijima and Ichihashi (1986) followed by a series of observations of these transformations in transition metals on oxides and carbon (Smith, Petford-Long, Wallenberg and Bovin 1986, Wallenberg, Bovin, Petford-Long and Smith 1986, Malm, Bovin, Petford-Long and Smith 1988, Mitome, Tanishiro and Takyanagi 1989, Iijima and Ichihashi 1991, Bovin and Malm 1991) indicated analogous behaviour in small particles. Dundurs, Marks and Ajayan (1988) theoretically evaluated the energies of the decahedral MTP for various positions of the disclination and showed that the energy differences between the Sc and the Dc were indeed small. The extension of the idea of a configurational space of morphologies, where the particles transformed rapidly, led to the the construction of a 'phase map' of the morphologies as functions of temperature and size (Ajayan and Marks 1988). The map, while providing a possible interpretation for the formation of exceptionally large Ics in the electron diffracton studies by inert gas aggregation methods on unsupported Ag particles (Hall, Flueli, Monot and Borel 1991, Reinhard, Hall, Ugarte and Monot 1993) has not been rigorously verified by experiments. Several review articles detail the history of these developments (Ogawa and Ino 1971, Ajayan and Marks 1990, Marks and Doraiswamy 1994, Marks 1994, Uyeda 1991).

As is apparent from the real-time observations and the theoretical simulations, particles occupy a variety of morphologies which can be considered as local minima in potential energies in a configurational space (Marks 1983). The nucleation and

growth of the particles follow a trajectory in this space decided by the probabilities of the morphologies at a given time for the local conditions around the particle. In this sense, the particle morphologies are history-dependent, and any real attempt to decipher the evolution of particle morphologies would have to consider the entire configurational space or at least a section of the space for a given controlled set of conditions (Marks 1994).

At this juncture of studies on small particles there is a bewildering amount of information on small particles. However, all the experiments, except the inert gas aggregation methods (Renou and Gillet 1981, Hall *et al.* 1991, Reinhard *et al.* 1993, Reinhard, Berthoud, Ugarte, Hall and Monot 1994) and the static morphology study by Yagi, Takayanagi, Kobayashi and Honjo (1975), sample only single points of the configurational space. While the inert gas aggregation methods are more affected by conditions at the evaporation source and the gradient in conditions below it, experimental real-time information has been largely limited to short-time observations which only show the existence of structural transformation in small particles. Only two papers (Kizuka, Kachi and Tanaka 1993, Narayanaswamy and Marks 1993) identify and quantitatively differentiate the components of the real-time observations in small particles. Kizuka *et al.* (1993) focused on the orientation relationship between a fluctuating small Au particle and its substrate (MgO crystallite). Narayanaswamy and Marks (1993) showed that a fluctuating Au particle subjected to an electron beam has a high rate of rotations along with a much lower rate of transformations. In particular, real-time high-resolution electron microscopy (HREM) has not been used quantitatively to follow the time evolution of the transformations of a small particle for a range of sizes.

In this paper we report the results of a detailed real-time HREM analysis of the structural transformations of Au particles on a SiO substrate, and show for the first time that structurally fluctuating particles have preferred morphology regimes. A probability model based on the potential energies of the small particles is then developed to construct morphology maps of fluctuating small particles.

§ 2. Experimental methods

2.1. *Sample preparation and data reduction*

Samples were prepared by depositing small particles of Au onto crushed SiO at a vacuum of 2×10^{-6} Torr and then transferred to a Hitachi H-9000, 300 kV transmission electron microscope maintained at a typical vacuum of 10^{-7} Torr. The sample was then annealed in the microscope at a beam flux of $85\,A\,cm^{-2}$ to obtain well separated particles. The anneal also elevated the particles onto cup-like mounds of the substrate.

Particles on the edge of the SiO substrate parallel to the electron beam were used for further observations. The particles were excited into undergoing morphological transformations by varying the beam flux and their behaviour recorded in real time using a Sony EVO9800 Hi-8 video recorder connected to a fibre-optically coupled Gatan television camera. The images were captured at the standard NTSC rate of 30 frames per second and then transferred to a workstation through an image grabber for further analysis using SEMPER, an image processing program. Even though the fluxes required to initiate the process of morphological transformations are very high ($22\,A\,cm^{-2}$), the fluxes required to sustain it are much lower (Ajayan and Marks 1989). Particles smaller than 5 nm transformed between morphologies even at $3\,A\,cm^{-2}$, the minimum flux at which the particle fluctuations could be recorded. In

general, the substrate directly below the particles tends to form mound-like pillars. Higher fluxes led to very rapid movement and rotation of the particles which displaced them off the mounds. After being displaced off the mounds, the rate of structural transformations of the particles decreased until they once again rested on top of pillars. All observations to determine the relative probabilities were therefore conducted by first initiating the formation of pillars. Particles were observed only as long as they resided on the same pillar.

To ensure a good statistical count each observation lasted for more than 3 min. During this time several hundred image frames were recorded. These images were then analysed by using a data-reduction scheme. A basis set of good images was selected from each recording and competely characterized by using simulated images and experimental images obtained by earlier workers (Marks and Smith 1981, Buffat *et al.* 1991, Altenheim, Giorgio, Urban and Weiss 1991, Giorgio, Nihoul, Urban and Sack-Kongehl 1992, Giorgio, Chapon, Henry and Nihoul 1993). Each basis set consisted of four distinct morphologies in various orientations, featureless structures were identified as indistinguishable, and structures with features that could not be classified were categorized as unknowns. Samples of the morphologies isolated are shown in fig. 1.

The entire recording for that particle size was then processed frame-by-frame by matching all the images with the characterized basis set. The images were matched by comparing overall particle morphology, faceting and re-entrant faces. Cross-correlation filtering with a gaussian, Fourier filtering and power spectra of single-frame images were used to enhance the visibility of any fringes in the particle.

2.2. *Experimental results*

A typical set of time sequence series obtained by the data reduction scheme is shown in fig. 2. The particle transformations do not show any order of preference; that is, any of the morphologies can form from any other of the morphologies in the basis set. The entire basis set is covered in a few seconds for even the lowest flux of observation. The sequences also show that increasing the beam flux increases the rate of transformation between morphologies. From these observations it can be directly inferred that the electron beam provides an external driving energy for the particle to surmount the activation energy barriers between the different morphologies.

A better representation of the kinetics of morphology transformations can be extracted from the time sequence series in terms of the mean residence time t_m in a morphology which is directly related to the activation energy barrier as

$$t_m = \nu \exp\left(\frac{-G}{kT}\right), \tag{1}$$

where ν is the number of attempts made by the particle to overcome the activation barrier G at temperature T. k is the Boltzmann constant.

The mean residence times for all the morphologies show a very weak dependence on the beam flux (fig. 3). The mean residence times extracted from time sequence series are shown in fig. 4 for constant fluxes. The Ic mean residence time shows a size invariance, whereas the Sc and the Dc mean residence times increase with size.

The experimental probability of occurrence of a morphology was measured as the fractional residence time, which can be obtained as

Fig. 1.

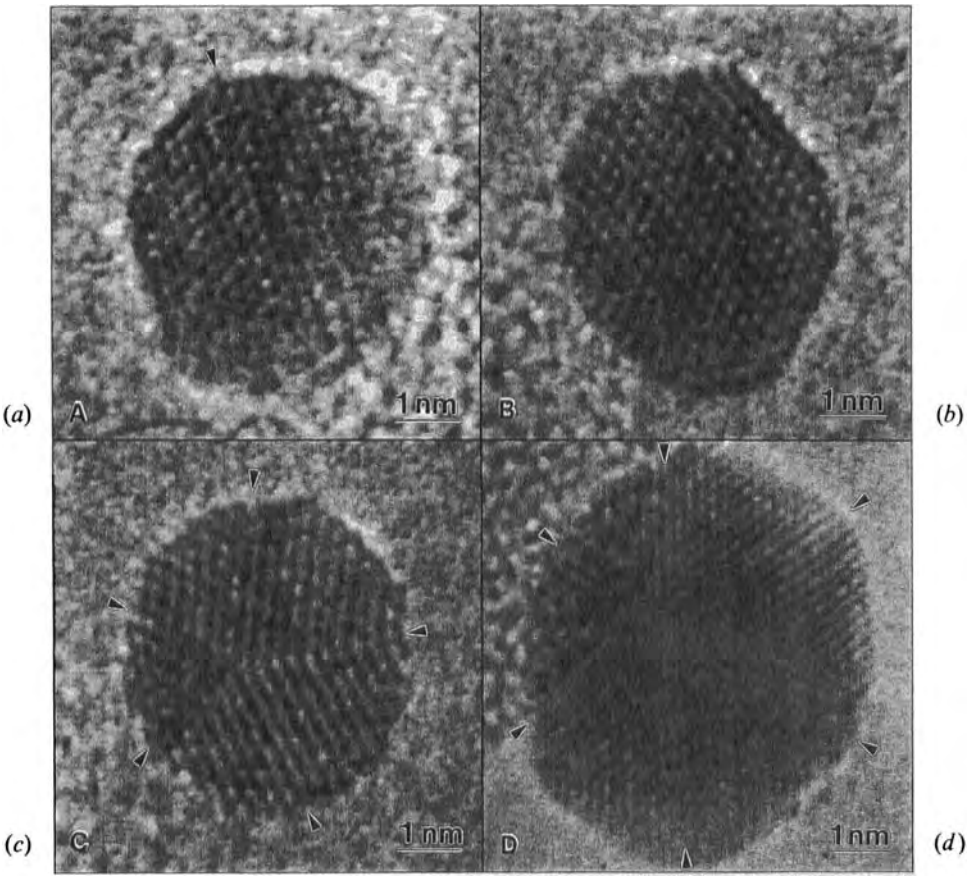

Samples of the basis set morphologies used in the data reduction scheme: (*a*) single twin, (*b*) single crystal, (*c*) decahedral MTP, (*d*) icosahedral MTP. Arrows indicate twinned regions.

$$F_{\text{res}} = \frac{T_{\text{morph}}}{\sum T_{\text{morph}}}, \tag{2}$$

from the mean residence times. The summation is over all the morphologies characterized in the basis set.

This probability is plotted in fig. 5 as a function of the particle size. The MTPs and the single crystals occur over the entire range of observations. Interestingly, the single-crystal morphology shows a high abundance at all sizes and shows an increase with size. The decahedral MTP follows a similar trend; however, the relative abundance is much smaller. The icosahedral MTP shows a decrease in probability with size, leading to a broad transition range between 5·5 and 7·0 nm in which the icosahedral MTP and the decahedral MTP have almost equal probabilities.

These experimental results show a predominance of Sc at all sizes and also that the Ics are not confined to very small sizes, which are in contradiction to those expected from the phase map constructed by Ajayan and Marks (1988). The gradual increase

Fig. 2.

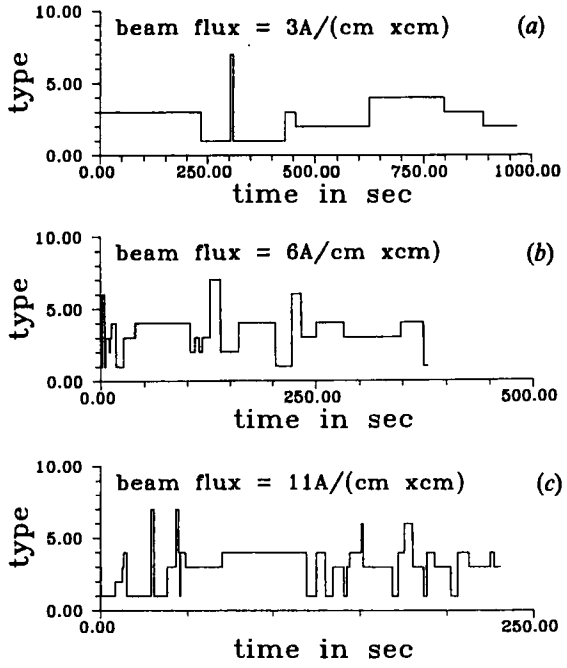

Time sequence evolution of the morphologies for a 6 nm particle at: (*a*) 3 A cm^{-2}, (*b*) 6 A cm^{-2}, (*c*) 11 A cm^{-2}. Each type of morphology has been assigned an arbitrary value. 1 is for the decahedral MTP, 2 for icosahedral MTP, 3 for single crystal, 4 for single twins, 6 for indistinguishable, and 7 for unknowns. The *x*-axis represents the time spent in a morphology.

Fig. 3.

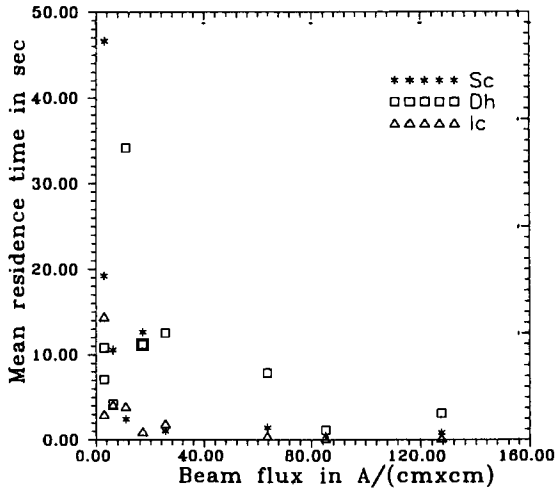

Mean residence time plotted as a function of the beam flux.

Fig. 4.

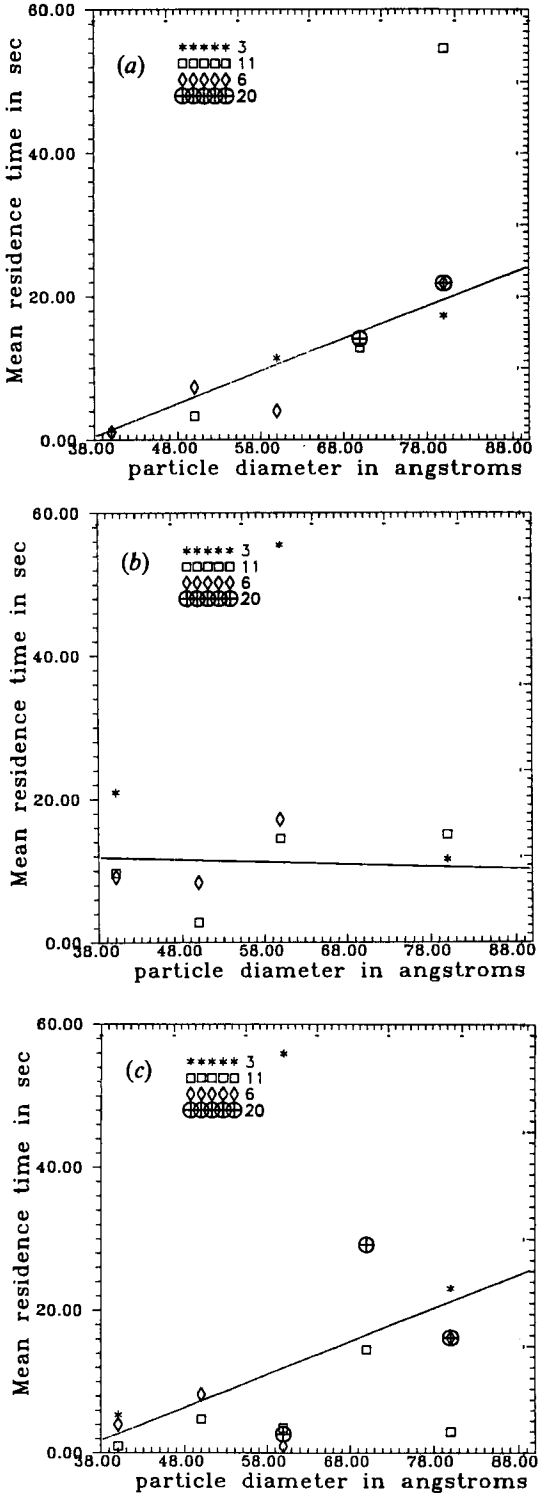

Mean residence time plotted as a function of particle diameter in angstroms at constant fluxes of 3, 6, 11 and 20 A cm^{-2}, respectively, for three morphologies: (*a*) Dc, (*b*) Ic, (*c*) Sc. The lines are drawn to guide the eye in observing the trend.

Fig. 5.

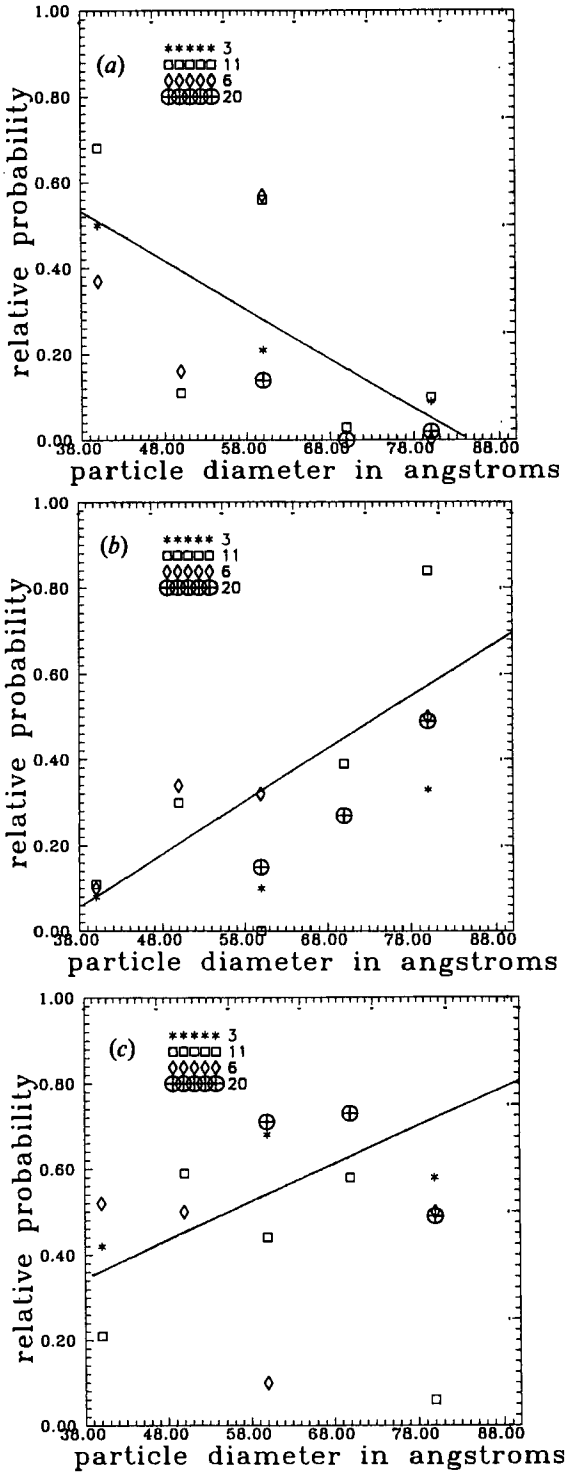

Experimental probability measured as fractional residence time in per cent plotted as a function of particle diameter in angstroms for beam fluxes of 3, 6, 11 and 20 A cm^{-2}, respectively, shows the downward trend in probability for: (*a*) Ic, and the upward trends for (*b*) Dc and (*c*) Sc. The lines help guide the eye in observing the trend.

of the decahedral phase with size over a large regime is also unexpected in terms of the phase map. However, the phase map does show a qualitative agreement with the electron diffraction studies on unsupported small particles of Ag (Hall *et al.* 1991) and Au (Patil, Paithankar, Otsuka and Andres 1993) produced by inert gas aggregation. In these experiments the morphology is strongly affected by the temperature and saturation conditions at the evaporation source which was maintained at temperatures greater than 1200 K. Such high temperatures cannot be produced by the interaction of the electron beam with the small particles at the low fluxes used in our experimental analysis. The temperature at the particle due to the electron beam has been calculated by several workers (Gale and Hale 1961, Fisher 1970, Rez and Glaisher 1991) and it is now accepted that the beam heating is very small and the temperature rise is less than 100 K.

§3. Analytical model

3.1. *Derivation of the analytical model*

In light of all the experimental results, it is clear that the phase map requires further refinement before being applicable as a predictive tool. The remainder of the paper will be devoted to the development of a morphology map based on an approach similar to that used by Ajayan and Marks (1988) and we will delineate regimes of dominance of the various morphologies in terms of the probabilities obtained from total energies of particle morphologies.

In the continuum elasticity approach, the total energy of a small particle is determined by the gain in surface energy compensated for by the strain energies of the particle. Following Howie and Marks (1984), the total energy can be reduced as a function of the volume, shape and strain parameters as

$$E_{\text{tot}} = (\varepsilon_{\text{w}} + \varepsilon_{\text{g}})\gamma_{111} V^{2/3} + W_{\text{D}} V + \varepsilon_{\text{gs}} V^{1/3}, \tag{3}$$

where ε_{w} is a shape-dependent parameter, ε_{D} is the strain dependent parameter, t_{gs} is the contribution to the surface energy due to the surface stress tensor (arising from strain in the particle) and ε_{g} is the strain energy due to surface stress at the surface. ε_{w}, a dimensionless parameter, is determined only by the external shape of the unstrained particle and includes the energy contributions from the external facets and the twin boundary energies. Using the modified Wulff construction (Marks 1983) the parameter can be determined as

$$\varepsilon_{\text{w}} = \frac{1}{\gamma_{111}} \frac{\int \gamma_{\text{s}} \, \mathrm{d}S}{(\int \mathrm{d}V)^{2/3}}, \tag{4}$$

where γ_{111} is the surface energy per unit area of a (111) facet and γ is the unstrained surface energy of the particle (see Marks (1993) for the expressions of ε_{w} for various morphologies).

The surface energy is further relaxed by the surface stress contribution arising from the internal elastic strain fields. The major contribution to the internal elastic strain field in a MTP is due to the closing of the angular misfit within the MTP. The total internal strain energy per unit volume of a decahedral MTP (Howie and Marks 1984) is

$$W_{\text{D}} = \frac{\mu \varepsilon_{\text{d}}^2}{4(1-\nu)}, \tag{5}$$

where ε_d is the angular deficit strain of a decahedral MTP (0·0205), μ is the shear modulus and ν is the Poisson ratio. For an Ic as developed by Howie and Marks (1984)

$$W_D = 2\mu\varepsilon_d^2(1+\nu)/(1-\nu). \tag{6}$$

The internal strain introduces a strain at the surface. The additional correction term due to this strain is

$$\varepsilon_g = g e_s \tag{7}$$

where g denotes the surface stress tensor which describes the strain variation of the surface energy to the first order, and e_s, the mean strain at the surface, is

$$e_s = (2/9)\varepsilon_d, \tag{8}$$

for icosahedral MTPs, and

$$e_s = (2/3)\varepsilon_d, \tag{9}$$

for decahedral MTPs.

The surface stress will also exert an expansive or compressive load on the surface, independent of any equilibrated stresses that already exists in the particle owing to internal distortions. By assuming a homogeneous strain, an additional energy change of

$$\varepsilon_{gs} = \frac{-\varepsilon_w^2 g^2 \gamma_{111} V^{1/3}}{3}\left(\frac{1-2\nu}{2}\right), \tag{10}$$

is incorporated in the evaluation of the surface energy contributions.

To derive the Gibbs free energy change G from the potential energies derived above, it is necessary to include the entropy of the energy terms. The entropy of the surface free energy change results from the entropy of the surface stresses, the entropy due to the anisotropic nature of the surface. The entropic change in strain energy is a direct consequence of the temperature dependence of the elastic moduli. The Gibbs free energy can then be expressed by the standard thermodynamic expression as

$$G = E_{tot} - TS. \tag{11}$$

From the Gibbs free energies, the relative probabilities of the morphologies are

$$P_{rel} = \frac{P_{morph}}{\Sigma P_{morph}} \tag{12}$$

where

$$P_{morph} = \exp\left(\frac{-G}{kT+\Delta E}\right) \tag{13}$$

where ΔE is the external driving energy (due to energy transfer from the electron beam) in addition to the temperature.

Small particles also show a depression in melting point with decreasing size. This effect was included in the model by using the values determined by Buffat and Borel (1976) as the upper limit of the solid phase of a small particle.

3.2. *Analytical model results*

From the relative probabilities and the depression in melting point one can construct a morphology map of the particles, namely the relative probabilities of occurrence as functions of temperature and size.

A typical morphology map constructed from the above model for Au is shown in fig. 6. The constants used in the evaluation of the relative probabilities of Au are tabulated in the table. A driving energy of 10 eV was applied to the particles with a surface stress of $0{\cdot}8\ \mathrm{N\,m^{-2}}$ and an anisotropy of $1{\cdot}15\ ((\gamma_{100}=1{\cdot}15\gamma_{111}))$ to obtain fig. 6. At all driving energies, anisotropy and surface stress, the Dcs appear only as secondary morphologies. The Ics dominate at lower sizes, whereas the Scs are predominant at larger sizes.

The variation of probabilities of the morphologies, at a particle temperature of 300 K, is shown in fig. 7 as a function of size and driving energy. On addition of an external driving energy of only 3 eV, the Dc probability begins to rise. An increase of the driving energy to 10 eV leads to a considerable increase in the Dc probability. Such energies can be provided by the electron beam. Rez and Glaisher (1991), assuming a linear dependence of the energy deposited per incident electron with particle radius, showed that a particle 4 nm in diameter can acquire an energy of 4 eV. It should be noted that the energy deposited in a particle is far less than that required to melt it. Increasing the beam flux, however, increases the rate of transformations between the morphologies (as shown in the time sequence) by decreasing the energy differences between the morphologies. However, at these conditions the beam energies rapidly increase the rotations, and as a consequence the particles tend to migrate randomly on the substrate.

Another factor that influences the regimes of dominance of morphologies is the surface stress. The variation of the relative probabilities with surface stress is shown in fig. 8 at a constant temperature of 300 K and at a driving energy of 10 eV. There is a significant change in the relative probabilities of the morphologies with a change in the surface stress. Decreasing the surface stress to zero decreases the decahedral MTPs and the single crystals. The relative probability of finding a decahedral MTP also shifts more towards smaller sizes. On the other hand, the icosahedral MTP becomes more dominant with decreasing surface stress. Most metal clusters are known to have lattice contractions, which are explained as an effect of the increase in pressure inside the particles that arises owing to their positive surface stress (Solliard and Flueli 1985). Unfortunately, there is no accurate estimate of the surface stress, owing to its extreme sensitivity to experimental conditions, and most tabulated values in the literature are derived from isotropic bulk surface tension values.

Finally, the effect of the anisotropy of the particle is illustrated in fig. 9 at a constant temperature of 300 K and a driving force of 10 eV. Higher anisotropy leads to more favourable conditions for the stability of Ics. Dcs, on the other hand, have the maximum probability only at intermediate anisotropies.

§4. Discussion

The data acquired from the experiment can be directly related to the relative probabilities from the standard equations and

$$F_{\mathrm{res}}=\frac{t_{\mathrm{morph}}}{\Sigma t_{\mathrm{morph}}}\propto\frac{P_{\mathrm{morph}}}{\Sigma P_{\mathrm{morph}}}=P_{\mathrm{rel}}. \tag{14}$$

The model shows a general agreement with the relative probabilities obtained from the experiment. The best fit is seen to occur at a driving energy of 10 eV and a surface stress of $0{\cdot}8\ \mathrm{N\,m^{-2}}$ at an anisotropy of $\gamma_{100}=1{\cdot}15\gamma_{111}$ (fig. 10).

The agreement is more in the reflection of a trend rather than in the fit with the data. A more accurate fit would require the collection of a much larger number of

Fig. 6.

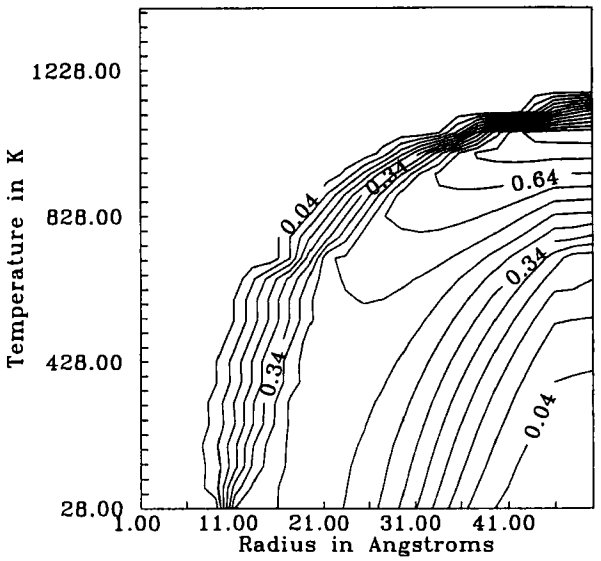

(*a*)

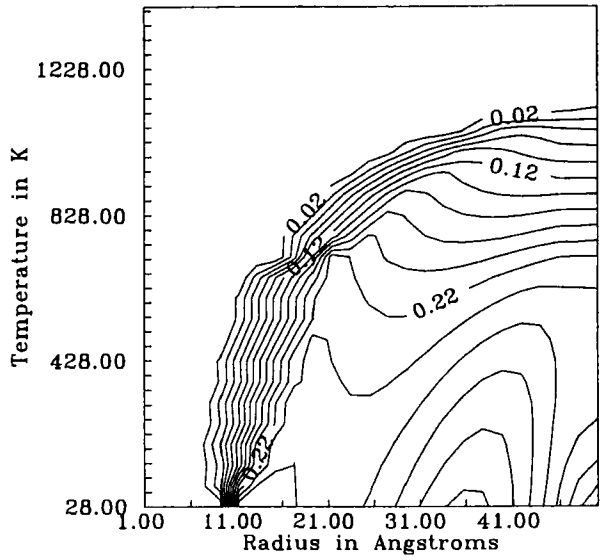

(*b*)

Fig. 6. *Continued*

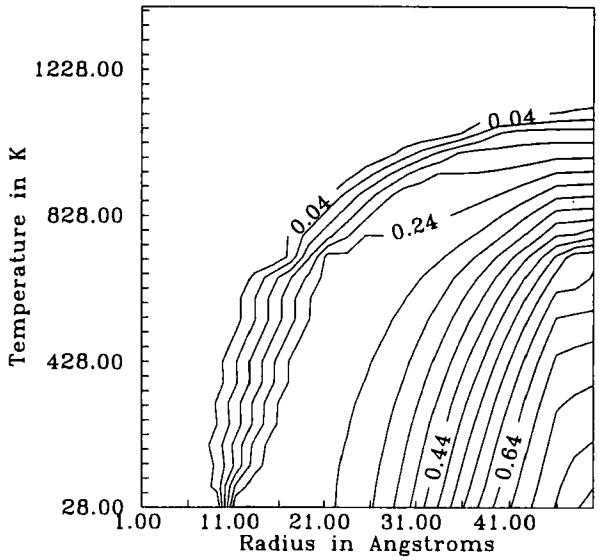

(*c*)

Typical set of relative probability maps of the morphologies at a driving energy of 10 eV and the remaining constants determined from the standard values tabulated in the table. The contour lines define the probability as a function of the temperature and particle radius. The depression in melting point (Buffat and Borel 1976) curve separates the liquid and solid phases: (*a*) Ic relative probability map, (*b*) Dc relative probability map, (*c*) Sc relative probability map.

Standard values of the various parameters used in the calculation of the morphology map of Au.

Bulk melting point (Hultgren *et al.* 1973)	1336 K
Bulk enthalpy of melting (Kristyan and Olson 1991)	12×10^3 J mol^{-1}
111 surface energy (Howie and Marks 1984)	2·26 J m^{-2}
100 surface energy (Howie and Marks 1984)	2·71 J m^{-2}
Liquid surface energy (Buffat and Borel 1976)	1·135 J m^{-2}
111 surface entropy (Linford 1973)	$1{\cdot}2 \times 10^{-3}$ J(m^{2}K^{-1})$^{-1}$
Surface stress (Keene 1993)	1·1 N m^{-1}
Surface stress entropy (Keene 1993)	-1×10^{-3} N(mK)$^{-1}$

data points. However, the process is prohibitively time consuming. Each of the experimental data points presented in the results were averaged over a range of 1 nm at each particle size, and each data point is in fact the average of six different sequences of observations. The averaging was necessitated by the small amount of variability in the particle diameter and deviation from a spherical shape during the process of morphology transformations. The particle transformation rate is also affected by the height and width of the substrate pillars which varied by small amounts during each observation. Although an amorphous substrate with a minimal

Fig. 7.

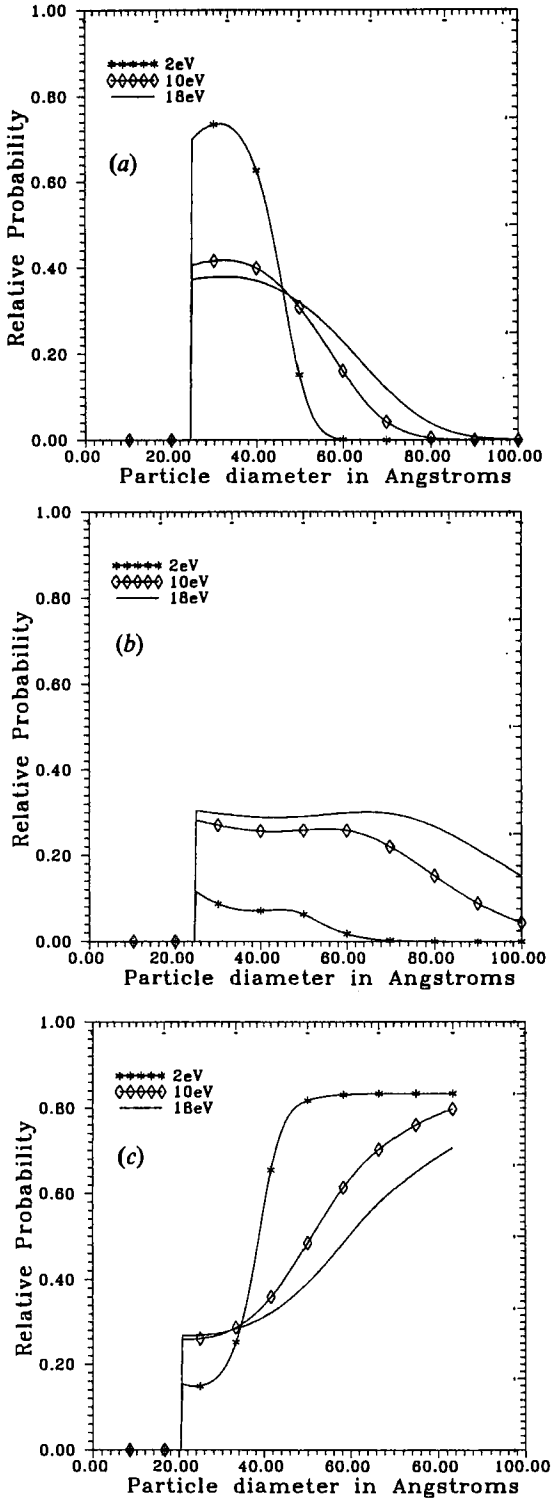

Variation of the relative probability of: (*a*) Ic, (*b*) Dc, (*c*) Sc, with driving energy illustrated for driving energies of 2, 10 and 18 eV. The graphs are isothermal sections at 300 K of a relative probability versus temperature, particle diameter in angstroms map.

Fig. 8.

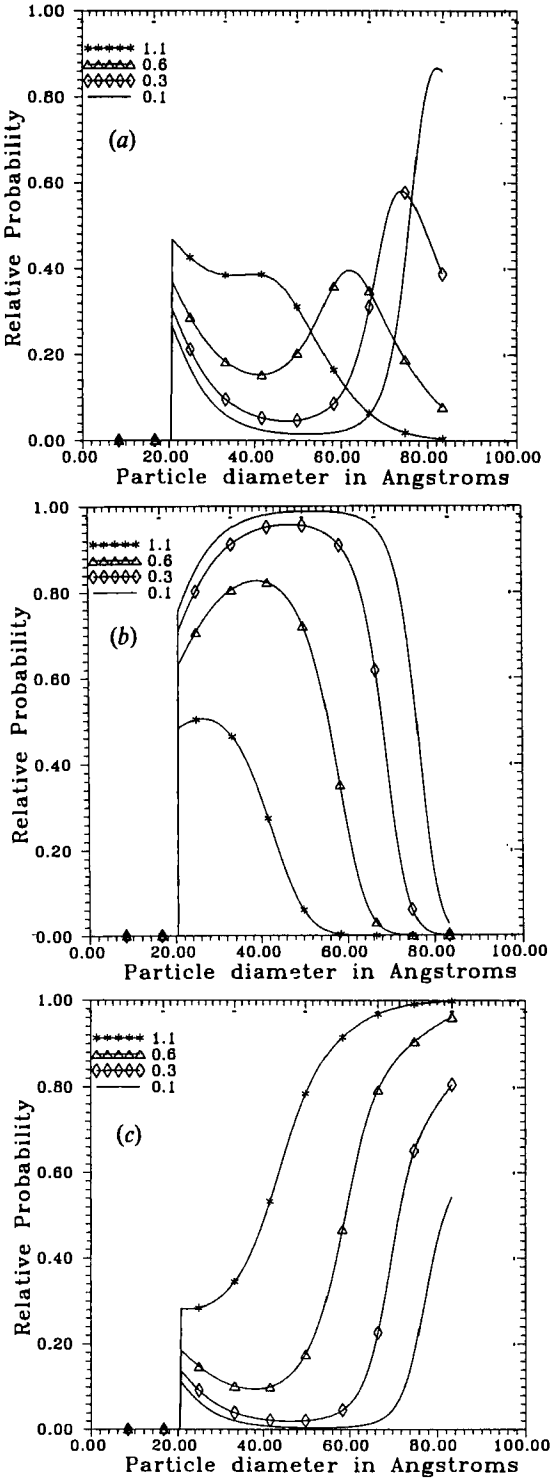

Isothermal section at 300 K of a three-dimensional morphology map of relative probability versus temperature, particle diameter in angstroms illustrating the variation of the relative probability with surfce stress (in $N\,m^{-2}$) for: (*a*) Dc, (*b*) Ic, (*c*) Sc, at a driving energy of 10 eV.

Fig. 9.

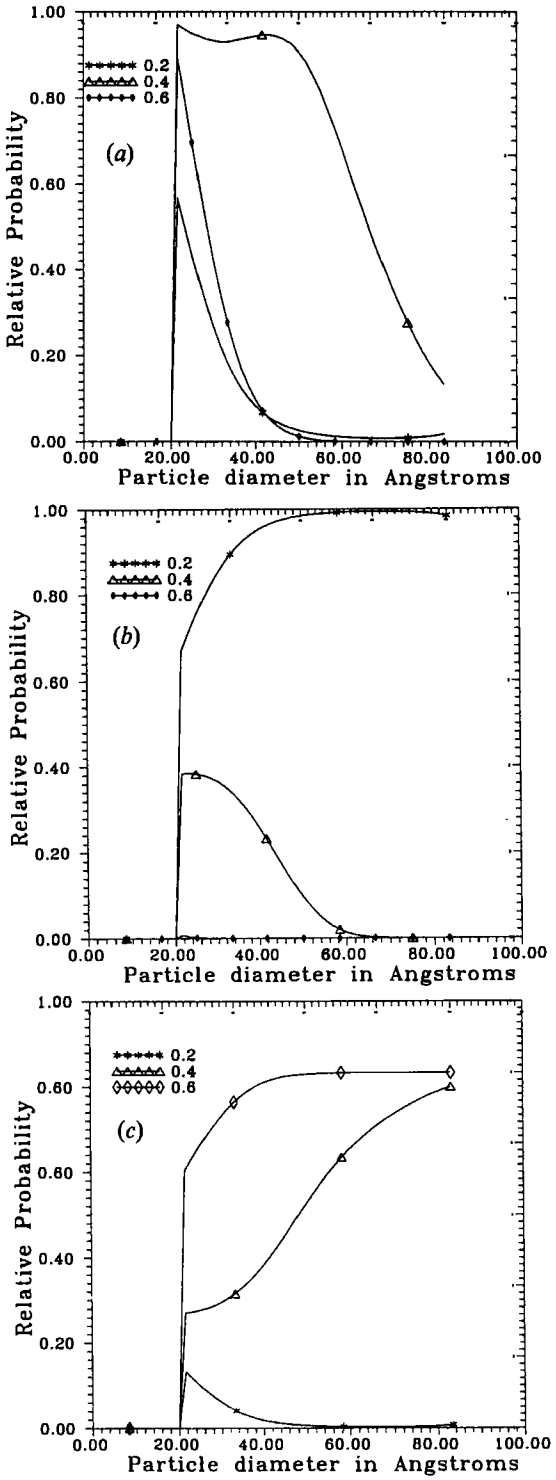

Isothermal section at 300 K of a three-dimensional morphology map of relative probability versus temperature, particle diameter in angstroms illustrating the variation of the relative probability with anisotropy (defined as $\beta = 1 - [\gamma_{100}/(\sqrt{3}\gamma_{111})]$) for: (*a*) Dc, (*b*) Ic, (*c*) Sc, at a driving energy of 10 eV.

Fig. 10.

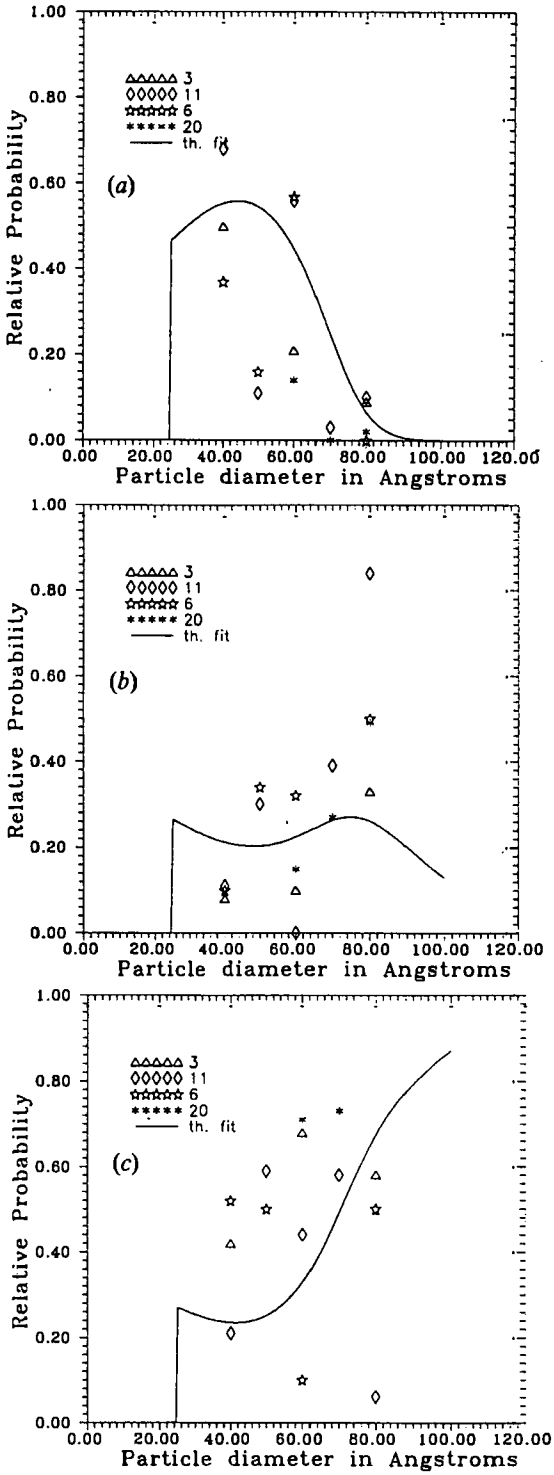

Best fit morphology sections of: (*a*) Ic, (*b*) Dc, (*c*) Sc, at 300 K of the probability model compared with the experimental data reveals the crossover regime centred at 6·5 nm. The surface stress is 0·8 N m^{-2} and the anisotropy is such that $\gamma_{100} = 1{\cdot}15\gamma_{111}$ at a driving energy of 10 eV.

area of contact with the particle does reduce the effect of the substrate, it does not eliminate the interaction. The effect of the interface is more dramatically observed by differences between our experimental observations and a similar time analysis conducted by Kizuka *et al.* (1993) for Au particles on MgO crystallites. They restricted their observations to only one particle size, 2 nm, at a beam flux of $3\,A\,cm^{-2}$, and found that the time of residence was split as 36, 18, 11 and 1% for the Dc, Sc, single twin and Ic, respectively. In our observations, a similar particle at the same beam flux showed an Ic dominance, followed by the Sc, and then the Dc. The difference in the observations can be accounted for by a shift in the stability of Ic arising as a result of the additional strain introduced by the interfacial relationship with a crystalline substrate. Another piece of evidence which supports this hypothesis is the relatively small number of icosahedral MTPs found in Ag islands deposited onto Si(100)-2 × 1 (Doraiswamy, Jayaram and Marks 1994). However, when exposed to air the silicon surface oxidized into an amorphous interface and was accompanied by an increase in the number of Ics. Other investigations (Ajayan and Marks 1989, Giorgio, Chapon, Henry, Nihoul and Penisson 1991, Giorgio *et al.* 1993) have also shown the effect of adhesion of the particle to the substrate on the particle morphology.

One of the trends observed in the morphology maps is the role of the driving energy. Larger energies, while increasing the rates of transformations, increase the relative probability of Dcs. The increase in energy also causes the Ic probability to broaden to larger sizes, and it decreases the Sc relative probability. The morphology maps have been calculated by assuming the MTPs to be perfect in shape. Experimental observations show a number of MTP structures in which the disclination is much closer to the edge. Such structures have a much lower activation barrier (Dundurs *et al.* 1988) and the Dcs would have a higher occurrence than those calculated here. As a consequence, small energy fluctuations cause larger changes in the morphology populations at low temperatures than at higher temperatures. This could be a probable cause for the conflicting reports of the number of MTPs observed in static morphology analyses, which vary from a few (Avery and Sanders 1970) to 95% (Solliard *et al.* 1976, Renou and Gillet 1981, Renou and Rudra 1985) of the total number of observed particles. A discussion of the various possible conditions resulting from the variations in the driving energy can be found in the review article by Marks (1994).

The particle morphologies are also strongly affected by the surface stress and anisotropy. Both of these parameters are very sensitive to the environment, and the production of a large number of a type of morphology can be achieved by a simple change of these two parameters. Although the role of the surface stress has not been experimentally confirmed, there is substantial evidence (for example, Stephanopoulos, Wong and Schmidt (1977)) for the role of the gaseous environment in changing the facetting conditions in a particle. However, further examination of the role of these parameters in controlled environments is required to quantify the effects.

The morphology maps also show that MTPs decrease at large sizes only at very high temperatures, which is consistent with experimental observations (for example, Patil *et al.* (1993)). Therefore the formations of MTPs is a low-temperature phenomenon, and the fluctuations in small particles can occur at low temperatures. The model and the experimental results thus reaffirm the hypothesis that structural fluctuations of a small particle in the presence of an electron beam are due to the intrinsic instability of the particles, rather than to violent processes such as rapid melting and

recrystallization. An interesting point observed in the morphology model is that it is not the overall temperature, but the small random energy fluctuations around the overall energy, that affects the morphology fluctuations. The overall energy plays a role only in the softening of the activation energy barriers, but the random energy fluctuations carry the particles over the activation barriers. The model thus offers an explanation of the role of the electron beam in the fluctuations observed by Miki-Yoshida, Tehuacanero and Jose-Yacaman (1992) at high temperatures. They also noted that the electron beam did not affect the particles at low temperatures, at which the activation energy barrier would be higher than the random energy fluctuation produced by the electron beam.

§ 5. Conclusions

In summary, results of the experimental analysis provide for the first time evidence that a fluctuating small particle continues to follow the thermodynamic morphology map, and excursions into other local minima have time lengths proportional to the relative probabilities of the minima. The particles in the range 2–9 nm show a mixed morphology of Dc, Ic and Sc. Scs have the highest relative probability of occurrence at all sizes. The abundance of the Ics and Dcs shows a crossover size, with the Ics being more dominant at smaller sizes.

Acknowledgments

We gratefully acknowledge support from the NSF on grant number DMR-9214505/001.

References

Ajayan, P. M., and Marks, L. D., 1988, *Phys. Rev. Lett.*, **60,** 585; 1989, *Ibid.*, **63,** 279; 1990, *Phase Transitions*, **24,** 229.

Allpress, J. G., and Sanders, J. V., 1967, *Surface Sci.*, **7,** 1.

Altenheim, C., Giorgio, S., Urban, J., and Weiss, K., 1991, *Z. Phys.* D, **19,** 303.

Avery, N. R., and Sanders, J. V., 1970, *J. Catal.*, **18,** 129.

Badzian, A. R., Badzian, T., Roy, R., Messier, R., and Spear, K. R., 1988, *Mater. Res. Bull.*, **23,** 531.

Bagley, B. G., 1965, *Nature*, **208,** 674.

Barry, J. C., Bursill, L. A., and Sanders, J. V., 1985, *Aust. J. Phys.*, **38,** 437.

Berry, R. S., 1990, *J. chem. Soc. Farad. Trans.*, **86,** 2343.

Bovin, J. O., and Malm, J. O., 1991, *Z. Phys.* D, **19,** 293.

Buffat, P. A., and Borel, J., 1976, *Phys. Rev.* B, **13,** 2287.

Buffat, P. A., Flueli, M., Spycher, R., Stadelmann, P., and Borel, J. P., 1991, *Faraday Discuss.*, **92,** 173.

Cleveland, C. L., and Landman, U., 1991, *J. chem. Phys.*, **94,** 7376.

Dahmen, U., and Westmacott, K. H., 1986, *Science*, **233,** 875.

Doraiswamy, N., Jayaram, G., and Marks, L. D., 1994, *Phys. Rev. Lett.* (submitted).

Dundurs, J., Marks, L. D., and Ajayan, P. M., 1988, *Phil. Mag.* A, **57,** 605.

Farges, J., de Feraudy, M. F., Raoult, B., and Torchet, G., 1983, *J. chem. Phys.*, **78,** 5067; 1984, *Dynamics of Surfaces*, edited by B. Pullman, J. Jortner, A. Nitzan and B. Gerber, p. 425.

Fisher, S. B., 1970, *Rad. Effects*, **5,** 239.

Gai, P. L., Goringe, M. J., and Barry, J. C., 1986, *J. Microsc.*, **142,** 9.

Gale, B., and Hale, K. F., 1961, *Brit. J. appl. Phys.*, **12,** 115.

Gillet, E., and Gillet, M., 1972, *J. Cryst. Growth*, **13/14,** 212.

Giorgio, S., Chapon, C., Henry, C. R., and Nihoul, G., 1993, *Phil. Mag.* B, **67,** 773.

Giorgio, S., Chapon, C., Henry, C. R., Nihoul, G., and Penisson, J. M., 1991, *Phil. Mag.* A, **64,** 87.

GIORGIO, S., NIHOUL, G., URBAN, J., and SACK-KONGEHL, H., 1992, *Z. Phys.* D, **24,** 395.
HALL, B. D., FLUELI, M., MONOT, R., and BOREL, J. P., 1991, *Phys. Rev.* B, **43,** 3906.
HALUSKA, M., KUZMANY, H., VYBORNOV, M., ROGI, P., and FEJDI, P., 1993, *Appl. Phys.* A, **56,** 161.
HOARE, M. R., and PAL, P., 1971, *Adv. Phys.*, **20,** 161.
HOFMEISTER, H., BARDAMID, A. F., JUNGHANNS, T., and NEPIJKO, S. A., 1991, *Thin Solid Films*, **205,** 20.
HOWIE, A., and MARKS, L. D., 1984, *Phil. Mag.* A, **49,** 95.
HULTGREN, R., DESAI, P. R., HAWKINS, D. T., GLEISER, M., KELLEY, K. K., and WAGMAN, D. D., 1973, *Selected Values of the Thermodynamic Properties of the Elements* (Metals Park, Ohio: American Society for Metals).
IIJIMA, S., 1987, *Jap. J. appl. Phys.*, **26,** 365.
IIJIMA, S., and ICHIHASHI, T., 1986, *Phys. Rev. Lett.*, **56,** 616; 1991, *J. Inst. Metals.*, **31,** 582.
INO, S., 1966, *J. Phys. Soc. Jap.*, **21,** 346; 1969, *J. Phys. Soc. Jap.*, **27,** 941.
KEENE, B. J., 1993, *Inter. Metals Rev.*, **38,** 157.
KIZUKA, T., KACHI, T., and TANAKA, N., 1993, *Z. Phys.* D, **26,** S58.
KRISTYAN, S., and OLSON, J. A., 1991, *Surf. Sci. Lett.*, **255,** L562.
LINFORD, R. G., 1973, *Solid state surface Science II*, edited by M. Green (New York: Marcel Dekker), p. 1.
MACKAY, A. L., 1962, *Acta Crystallogr.*, **15,** 916.
MALM, J. O., BOVIN, J. O., PETFORD-LONG, A. K., and SMITH, D. J., 1988, *Angew. Chemie*, **27,** 555.
MARKS, L. D., 1980, *The structure of small silver particles.* PhD thesis, Cambridge, UK; 1983, *J. Cryst. Growth*, **61,** 556; 1994, *Rep. Prog. Phys.*, **57,** 603.
MARKS, L. D., and SMITH, D. J., 1981, *J. Cryst. Growth*, **54,** 425.
MARKS, L. D., and DORAISWAMY, N., 1994, *The Chemical Physics of Solid Surfaces and Heteregeneous Catalysis*, edited by D. A. King and D. P. Woodruff (Amsterdam: Elsevier).
MIKI-YOSHIDA, M., TEHUACANERO, S., and JOSE-YACAMAN, M., 1992, *Surf. Sci. Lett.*, **274,** L569.
MITOME, M., TANISHIRO, Y., and TAKYANAGI, K., 1989, *Z. Phys.* D, **12,** 45.
NARAYANASWAMY, D., and MARKS, L. D., 1993, *Z. Phys.* D, **26,** S70.
OGAWA, S., and INO, S., 1971, *Advances in Epitaxy and Endotaxy: Physical Problems of Epitaxy*, edited by H. G. Schneider and R. Volker (Leipzig: VEB Deutscher Verlag fur Grundstoffindustrie), p. 183.
PATIL, A. N., PAITHANKAR, D. Y., OTSUKA, N., and ANDRES, R. P., 1993, *Z. Phys.* D, **26,** 135.
REINHARD, D., BERTHOUD, P., UGARTE, D., HALL, B. D., and MONOT, R., 1994, *Phys. Low Dimens. Struct.*, **1,** 59.
REINHARD, D., HALL, B. D., UGARTE, D., and MONOT, R., 1993, *Z. Phys.* D, **26,** S76.
RENOU, A., and GILLET, M., 1981, *Surf. Sci.*, **106,** 27.
RENOU, A., and RUDRA, A., 1985, *Surf. Sci.*, **156,** 69.
REZ, P., and GLAISHER, R. W., 1991, *Ultramicroscopy*, **35,** 65.
SAITO, Y., YATSUYA, S., MIHAMA, K., and UYEDA, R., 1979, *Jap. J. appl. Phys.*, **17,** 1149.
SCHABES-RETCHKIMAN, P., GOMEZ, A., VAZQUEZ-POLO, G., and JOSE-YACAMAN, M., 1984, *J. vac. Sci. Technol.* A, **2,** 22.
SMITH, D. J., PETFORD-LONG, A. K., WALLENBERG, L. R., and BOVIN, J. O., 1986, *Science*, **233,** 872.
STEPHANOPOULOS, M. F., WONG, S., and SCHMIDT, L. D., 1977, *J. Catal.*, **49,** 51.
SOLLIARD, C., BUFFAT, P., and FAES, F., 1976, *J. Cryst. Growth*, **32,** 123.
SOLLIARD, C., and FLUELI, M., 1985, *Surf. Sci.*, **156,** 487.
THOLEN, A. R., 1981, *Surf. Sci.*, **106,** 70.
UYEDA, R., 1991, *Prog. Mater. Sci.*, **35,** 1.
WALLENBERG, L. R., BOVIN, J. O., PETFORD-LONG, A. K., and SMITH, D. J., 1986, *Ultramicroscopy*, **20,** 71.
YAGI, K., TAKAYANAGI, K., KOBAYASHI, K., and HONJO, G., 1975, *J. Cryst. Growth*, **28,** 117.
YANG, C. Y., 1979, *J. Cryst. Growth*, **47,** 274.
YANG, C. Y., YACAMAN, M. J., and HEINEMANN, K., 1979, *J. Cryst. Growth*, **47,** 283.